Journal of Zhejiang University-SCIENCE A (Applied Physics & Engineering)
ISSN 1673-565X (Print); ISSN 1862-1775 (Online)
www.zju.edu.cn/jzus; www.springerlink.com
E-mail: jzus@zju.edu.cn

Rate dependence of ultra high toughness cementitious composite under direct tension*

He-dong LI, Shi-lang XU†‡

(*Institute of Advanced Engineering Structures and Materials, Zhejiang University, Hangzhou 310058, China*)

†E-mail: slxu@zju.edu.cn

Received Jan. 24, 2016; Revision accepted May 11, 2016; Crosschecked May 26, 2016

Abstract: Ultra high toughness cementitious composite (UHTCC) usually shows strain hardening and multiple cracking under static tension loads. In practice, structures could be exposed to high strain rates during an earthquake. Whether UHTCC can maintain its unique properties and provide high structural performance under seismic loading rates largely determines whether it can successfully fulfil its intended function. To determine the rate dependence of UHTCC, uniaxial tensile tests with strain rates ranging from 4×10^{-6} s^{-1} to 1×10^{-1} s^{-1} were conducted with thin plates. The experimental results showed that UHTCC had significant strain hardening and excellent multiple cracking properties under all the rates tested. The ultimate tensile strain lay in the range of 3.7% to 4.1% and was almost immune to the change in strain rates. The rate of 1×10^{-3} s^{-1} seemed to be a threshold for dynamic increase effects of the first crack tensile strength, elastic modulus, ultimate tensile strength, and energy absorption capability. When the strain rate was higher than the threshold, the dynamic increase effects became more pronounced. The energy absorption capability was much higher than that of concrete, and the average ultimate crack widths were controlled below 0.1 mm under all rates. Several fitting formulas were obtained based on the experimental results.

Key words: Ultra high toughness cementitious composite (UHTCC), Rate dependence, Direct tension, Strain hardening, Multiple cracking

http://dx.doi.org/10.1631/jzus.A1600031 **CLC number:** TU528.58

1 Introduction

As a type of high performance fiber-reinforced cementitious composite (HFRCC), ultra high toughness cementitious composite (UHTCC) was developed under the guidelines of criteria for the design of multiple cracking strain hardening composites proposed by Li and Leung (1992). UHTCC is often referred to as engineered cementitious composite (ECC) (Li and Kanda, 1998) or strain hardening cement-based composite (SHCC) (Boshoff and van Zijl, 2007). This type of material was developed to overcome the weaknesses of concrete, which include brittleness, low tensile deformability, low tensile strength, vulnerability to cracking, and the tendency of fine cracks to develop into wide cracks. It usually shows excellent multiple cracking strain hardening behavior, with ultimate tensile strain consistently above 3% and with a corresponding ultimate crack width below 0.1 mm. It can retain its full bearing capacity and integrity under direct tension until the strain reaches the ultimate tensile strain. UHTCC also has good deformation compatibility with steel bars (Fischer and Li, 2002), high compressive deformability compared with normal concrete (Fischer, 2002; Xu and Cai, 2010), ductile fracture characteristics (Li and Hashida, 1993; Li and Xu, 2011), and notch insensitivity (Li, 1997; Xu and Li,

‡ Corresponding author

* Project supported by the National Natural Science Foundation of China (No. 51478423), the Research Foundation of the Department of Education of Zhejiang Province, China (No. Y201226058), and the Research Fund for the Doctoral Program of Higher Education of China (No. 20130101120071)

ORCID: He-dong LI, http://orcid.org/0000-0002-0911-1976

© Zhejiang University and Springer-Verlag Berlin Heidelberg 2016

2009). All the above excellent properties seem to render UHTCC a potentially ideal material solution for earthquake resistant structures or elements. However, a key factor of structural properties under seismic loading is their behavior under high strain rates (typically in the range from 1×10^{-4} s^{-1} to 1×10^{-2} s^{-1}), but most of the properties described above were achieved under quasi-static conditions (strain rates typically in the range from 1×10^{-6} s^{-1} to 1×10^{-5} s^{-1}). Among all the properties of UHTCC, the tensile response is the most important. Concrete is strain rate dependent in terms of its tensile strength, tensile elastic modulus, and ultimate tensile strain (Reinhardt, 1985; Rossi *et al*., 1994; Ross *et al*., 1995; Malvar and Ross, 1998; Xiao *et al*., 2001; Yan *et al*., 2005). The respective properties of UHTCC will largely determine its suitability in seismic and protective engineering applications.

There have been plenty of studies on the rate dependence of the tensile response of cementitious composites, but only a few studies on that of multiple cracking strain hardening cementitious composites. Among the limited studies, different and even conflicting conclusions were drawn. Maalej *et al.* (2005) investigated tensile strain rate effects on hybrid fiber ECC (steel fiber and polyethylene fiber) using 300 mm×75 mm×15 mm coupon specimens with tensile strain rates ranging from 2×10^{-6} s^{-1} to 2×10^{-1} s^{-1}. A substantial increase in the ultimate tensile strength from 3.1 MPa to 6 MPa with increasing strain rate was reported. No obvious trend of variation of the tensile strain capability with changing strain rates was observed. Multiple cracking and strain hardening behaviors were also unaffected by changing strain rates. Yang and Li (2006) investigated polyvinyl alcohol (PVA) fiber ECC using 220 mm×75 mm×12.7 mm coupon specimens with tensile strain rates ranging from 10^{-5} s^{-1} to 10^{-1} s^{-1}. Tensile strength increased markedly while the tensile strain capacity decreased significantly with increasing strain rates. Tensile ductility reduced from 3% to 0.5% at the highest strain rate. Boshoff and van Zijl (2007) investigated PVA fiber ECC using thin dumbbell specimens with a cross section of 30 mm ×16 mm and strain rates ranging from 1.04×10^{-5} s^{-1} to 1.04×10^{-1} s^{-1}. Significant dynamic increase effects of ultimate tensile strength and first crack tensile strength were reported. Tensile ductility and elastic modulus were rate independent. Yang and Li (2012) reported different rate dependences of three different ECCs with 304.8 mm×76.2 mm×12.7 mm coupon specimens. Mechtcherine *et al*. (2011) studied the tensile properties of PVA-ECC under rates in the range of 1×10^{-5} s^{-1} to 50 s^{-1} and found the tensile strength and elastic modulus both showed significant dynamic increase effects, while the strain capacity showed a significant dynamic decrease effect when the strain rates were in the range of 1×10^{-5} s^{-1} to 1×10^{-2} s^{-1}. Douglas and Billington (2011) studied PVA-ECC cylinders with a diameter of 51 mm under direct tension, with strain rates ranging from 2×10^{-5} s^{-1} to 2×10^{-1} s^{-1}. Both the tensile strength and strain capacity were significantly affected by the increasing strain rates. The strength increased from 25% to 120% while the strain capability decreased by 50%–55% when the strain rates attained seismic levels. No multiple cracking was found at seismic rates. Douglas and Billington (2011) reported a strong geometry effect on the tensile properties of UHTCC, where significant multiple cracking strain hardening characteristics with an ultimate tensile strain of 3.35% were achieved with 305 mm×76 mm ×13 mm coupon specimens. They found much less multiple cracking and a much lower ultimate strain of 0.63% with cylindrical specimens. Fiber dispersion may be considered 2D in the thin coupon specimens and 3D in the cylinders. The much reduced strain hardening characteristics of UHTCC in 3D specimens seem to reduce the advantages of using UHTCC in seismic applications, since most of the fiber dispersion in the fiber-reinforced cementitious composites is thought to be 3D in practical applications. Fortunately, however, rapid developments in the precast industry, extrusion technology, and the so-called 3D printing techniques may help to realize 2D fiber distribution in practical seismic elements. This indicates that the introduction of 2D applications of UHTCC may be worthwhile. Therefore, further systematic experimental research on 2D UHTCC specimens is warranted.

In this paper, the rate dependence of UHTCC was investigated using thin coupon specimens with direct tensile strain rates ranging from quasi-static to seismic levels. The rate effects on the first crack tensile strength, first crack tensile strain, tensile elastic modulus, ultimate tensile strength, ultimate tensile

strain, strain hardening, and multiple cracking behavior were investigated. The results provide scientific evidence supporting the practical application of UHTCC in seismic engineering.

2 Experimental

2.1 Materials and specimens

Cementitious binders, fine silica sand, water, superplasticizer, and PVA fiber were used to produce the UHTCC. The cementitious binders were composed of ordinary Portland cement, fly ash, and silica fume. The super-plasticizer was of the polycarboxylate type. The PVA fiber was KURALON K-II REC 15 (Japan) with the properties given in Table 1. The fiber fraction was about 2% of the total volume of the composite.

Table 1 Properties of PVA fibres

Parameter	Value
Length (mm)	12
Diameter (μm)	39
Tensile strength (MPa)	1620
Elongation (%)	7
Tensile modulus (GPa)	42.8
Density (g/cm^3)	1.3

The UHTCC was mixed in a Hobart D340 mixer with the following steps in sequence: (1) put the dry cementitious binders and fine silica sand into the mixer and mix for about 1 min; (2) add water and mix for about 2 min; (3) add superplasticizer and mix for about 5 min until the fresh mortar shows good flowability and cohesiveness; (4) add all the PVA fibers manually and mix for about 5 min until uniform composite is achieved.

The dimensions of the direct tension specimens were 350 mm×50 mm×15 mm (Fig. 1). The specimens were cast in steel molds and vibrated for about 10 s. Three carbon fiber bundles, 125 mm in length and cut from epoxy-impregnated carbon textile, were embedded to reinforce each end of the specimens. After finishing treatment, the specimens were covered with glass boards to achieve a smooth hardened casting surface and prevent evaporation of water. Plastic sheets were used for further evaporation prevention. The specimens were demolded after 24 h and taken into the curing room (with the temperature controlled in the range of (20±3) °C and relative humidity higher than 90%) where they were cured until day 28. The specimens were then further cured in an indoor environment until being tested at days 42–45.

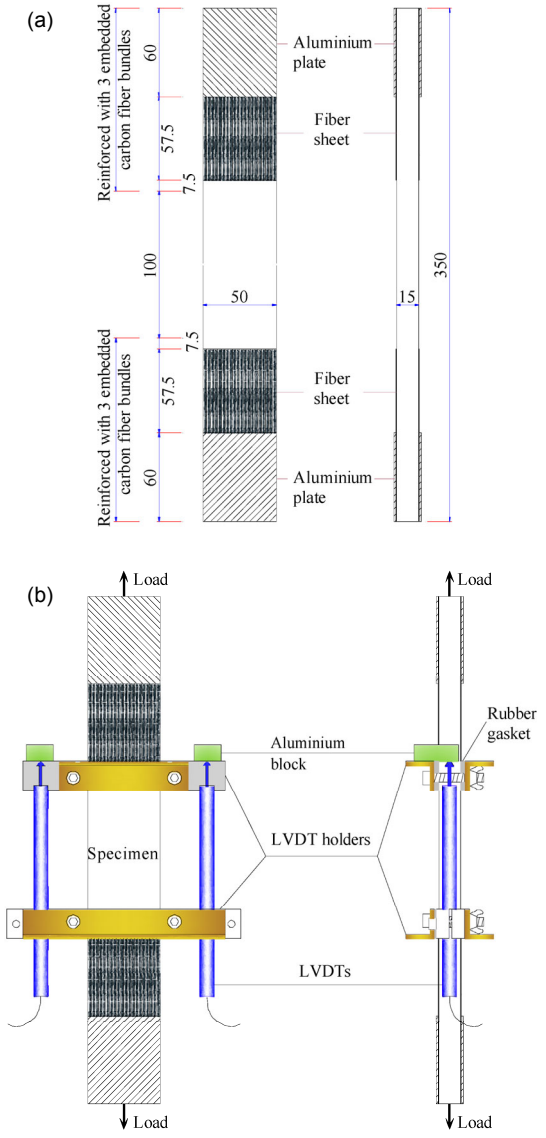


Fig. 1 Specimen and test method used in the direct tension test on UHTCC

(a) Dimensions of the specimen (unit: mm); (b) Schematic illustration of uniaxial tensile test. LVDT indicates linear variable differential transformer

2.2 Testing program

The direct tension tests were conducted in a 100 kN MTS 810 (USA) material testing machine

equipped with hydraulic wedge grips. Epoxy resin was used to glue basalt fiber sheets onto both ends of each specimen and aluminum plates onto the fiber sheets. The lengths of the fiber sheets and aluminum plates were 117.5 mm and 60 mm, respectively (Fig. 1). Meticulous attention was paid to guarantee that each pair of aluminum plates on the same side was parallel to the bottom surface of the specimen and in the same plane. The gluing operation was finished at least 12 h before the tests began. With the help of linear variable differential transformer (LVDT)-holders, two LVDTs were symmetrically installed to monitor the deformation of the specimen. The gauge length was 100 mm. To achieve a more accurate gauge length and eliminate possible damage to the specimen caused by the operation of fixing the LVDT holders, rubber gaskets with 2 mm-diameter metal wire passing through were used. The center-to-center spacing of the two metal wires along the length direction was the same as the gauge length. Care was taken to ensure alignment of the axis of the specimen and the testing machine when installing the specimen. The detailed configuration of the specimen is shown in Fig. 1. The tests were conducted under displacement control. Six different loading rates were applied: 0.024, 0.06, 0.6, 6, 60, and 600 mm/min. If elongation during the loading process was ignored, the loading rate could be converted into nominal strain rates of about 4×10^{-6}, 1×10^{-5}, 1×10^{-4}, 1×10^{-3}, 1×10^{-2}, and 1×10^{-1} s^{-1}, respectively. The deformations over the gauge length and the tensile load were both recorded using the dynamic data acquisition system of IMC.

3 Results and discussion

In the following analyses, the rate of 4×10^{-6} s^{-1} was considered as the quasi-static strain rate. The average ultimate crack spacing was evaluated as the original gauge length (i.e., 100 mm) divided by the number of through cracks in the whole gauge length region of the failed specimens. The average crack width was evaluated as the ultimate tensile strain multiplied by the original gauge length and divided by the number of through cracks in the whole gauge length region of the failed specimens. In the determination of average ultimate crack width and crack spacing, the elastic extension of the uncracked part of the specimens was neglected.

3.1 Direct tension experimental curves

The direct tension experimental curves are presented in Fig. 2. All the specimens showed significant strain hardening behavior under all strain rates tested. The appearance of the curves of the UHTCC was different from that of SHCC reported by Boshoff and van Zijl (2007). The difference lies in that the first crack tensile strengths were always lower than the ultimate tensile strength for UHTCC at all strain rates while this is not always the case for SHCC. Boshoff and van Zijl (2007) reported that the first crack tensile strength of SHCC increased faster than the ultimate tensile strength, and even exceeded it under the rate of 1.04×10^{-1} s^{-1}. This phenomenon may be due to the different test methods adopted and differences in detailed material composition.

The main tensile properties of UHTCC are summarized in Table 2. The tensile elastic modulus is the slope of the initial linear part of the stress versus strain curve of the specimen. Since slight initial torsion is prone to appear sometimes, only the data from the specimens without initial torsion were used to determine the tensile elastic modulus, the first crack tensile strength, and the first crack tensile strain. The existence of slight initial torsion was considered not to influence the ultimate tensile strain, ultimate tensile strength, average ultimate crack spacing, and average ultimate crack width.

3.2 Rate dependency of tensile elastic modulus

Fig. 3 (p.422) presents the ratio of dynamic to quasi-static tensile elastic modulus versus strain rate. The variation trend of the tensile elastic modulus of the UHTCC differs from that of the SHCC reported by Boshoff and van Zijl (2007). The tensile elastic modulus of the UHTCC tended to increase with the increasing strain rates instead of decreasing slightly as in the case of SHCC.

The modulus increased slowly when the rate was lower than 1×10^{-3} s^{-1}, and much more rapidly when the rate was higher than 1×10^{-3} s^{-1}. For simplicity, the dynamic increase factor of tensile elastic modulus can be modeled well as follows:

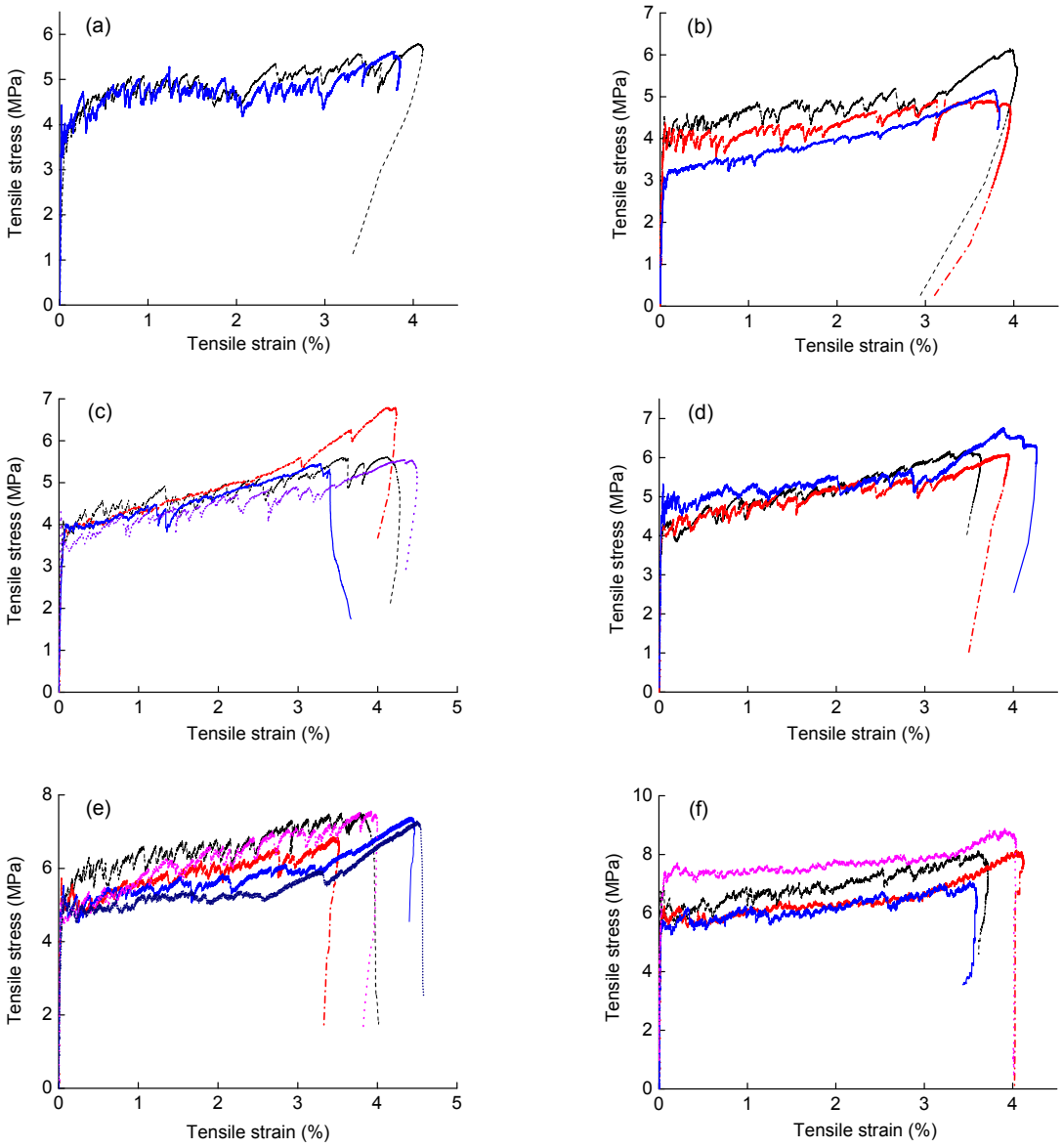


Fig. 2 Uniaxial tensile stress versus strain curves of UHTCC under different strain rates

(a) Under the strain rate of 4×10^{-6} s^{-1}; (b) Under the strain rate of 1×10^{-5} s^{-1}; (c) Under the strain rate of 1×10^{-4} s^{-1}; (d) Under the strain rate of 1×10^{-3} s^{-1}; (e) Under the strain rate of 1×10^{-2} s^{-1}; (f) Under the strain rate of 1×10^{-1} s^{-1}. The different curves in each figure denote specimens under the same strain rate

Table 2 Uniaxial tensile properties of UHTCC under different strain rates

Strain rate (s^{-1})	Tensile elastic modulus (GPa)	First crack tensile strain ($\times10^{-6}$)	First crack tensile strength (MPa)	Ultimate tensile strain (%)	Ultimate tensile strength (MPa)	Average ultimate crack space (mm)	Average ultimate crack width (μm)
4×10^{-6}	18.4	249	4.4	3.9	5.7	1.3	49
1×10^{-5}	–	–	–	3.9	5.5	2.4	94
1×10^{-4}	18.7	239	4.3	4.0	5.8	1.5	61
1×10^{-3}	20.2	205	4.1	3.8	6.3	1.7	63
1×10^{-2}	23.4	226	5.0	4.0	7.3	1.6	63
1×10^{-1}	27.5	215	5.9	3.7	8.0	1.4	54

$$E_t / E_{ts} = \begin{cases} 1.0 + 0.03341 \log \dfrac{\dot{\varepsilon}_t}{\dot{\varepsilon}_{ts}}, \\ \qquad 4\times10^{-6}\ \mathrm{s}^{-1} \le \dot{\varepsilon}_t \le 10^{-3.05798}\ \mathrm{s}^{-1}, \\ 0.614 + 0.19837 \log \dfrac{\dot{\varepsilon}_t}{\dot{\varepsilon}_{ts}}, \\ \qquad 10^{-3.05798}\ \mathrm{s}^{-1} < \dot{\varepsilon}_t \le 10^{-1}\ \mathrm{s}^{-1}, \end{cases} \quad (1)$$

where E_{ts} and $\dot{\varepsilon}_{ts}$ are the quasi-static tensile elastic modulus and the quasi-static tensile strain rate, $\dot{\varepsilon}_t$ is the tensile strain rate ranging from 4×10^{-6} s^{-1} to 1×10^{-1} s^{-1}, and E_t is the tensile elastic modulus under the strain rate of $\dot{\varepsilon}_t$.

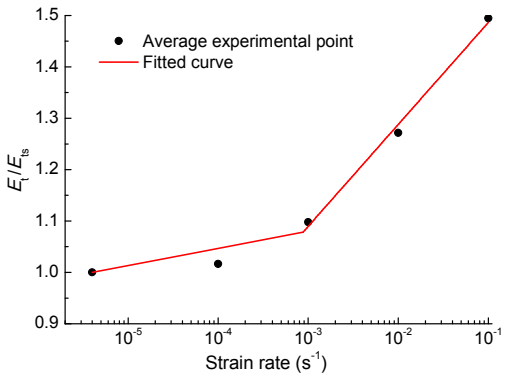


Fig. 3 Dynamic to quasi-static elastic modulus ratio versus strain rate curves

3.3 Rate dependency of multiple cracking properties

Typical photos of the multiple cracking of specimens under all strain rates are presented in Fig. 4. The saturated multiple cracking phenomenon appears under all rates. All the average crack spacings lie in the range of 1.0 to 2.5 mm, and the average crack widths are all less than 100 μm. This means that the PVA fibers can bridge the cracks well even under dynamic loads. In general, the multiple cracking properties of the UHTCC were rate independent. A tiny difference was observed in the detailed crack morphology between the quasi-static specimen and the specimens under higher loading rates. Initial cracking stage cracks in the static specimens were more tortuous than those under higher loading rates (Fig. 4). The more tortuous crack morphology may be due to the low loading rate of the static rate, which more easily permits the cracks to propagate along the weakest paths. The more tortuous cracks are also considered to permit more fibers to bridge the cracks and realize a more significant strain hardening effect at the beginning of the multiple cracking stage. This may explain why the curve under the static rates at the beginning of the multiple cracking stage was steeper than those under higher rates (Fig. 2).

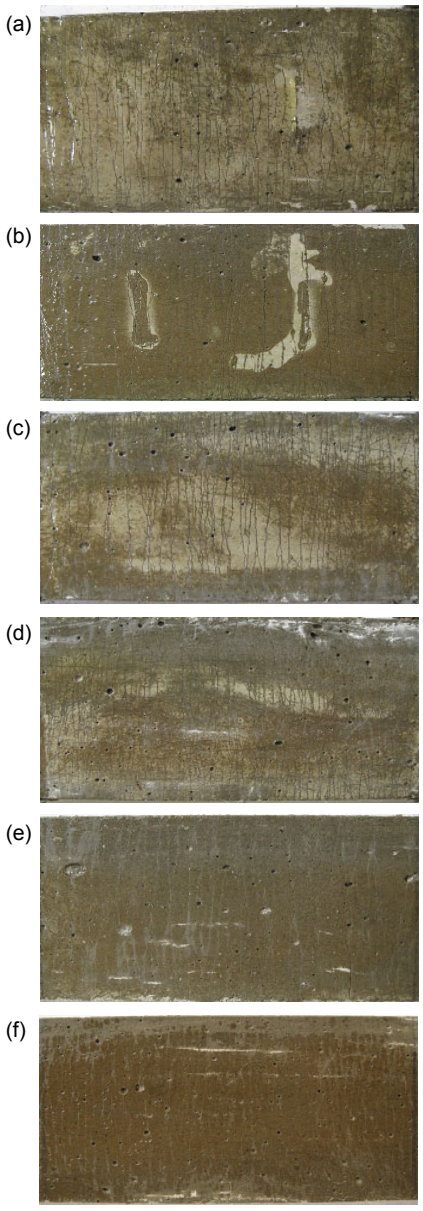


Fig. 4 Multiple cracking patterns under different strain rates

(a) Under the strain rate of 4×10^{-6} s^{-1}; (b) Under the strain rate of 1×10^{-5} s^{-1}; (c) Under the strain rate of 1×10^{-4} s^{-1}; (d) Under the strain rate of 1×10^{-3} s^{-1}; (e) Under the strain rate of 1×10^{-2} s^{-1}; (f) Under the strain rate of 1×10^{-1} s^{-1}

3.4 Rate dependencies of first crack tensile strength and strain

First crack tensile strain and strength correspond to the strain and stress, respectively, when the first crack appears. In the experimental curves, they correspond to the point where the initial linear portion ends. The ratio of the dynamic to static first crack tensile strain versus the strain rate is presented in Fig. 5. The first crack tensile strain is rate dependent. The dynamic decrease effect is clear: the first crack tensile strain tended to decrease continuously with increasing strain rate, except at the strain rate of 1×10^{-3} s^{-1} where it clearly deviated from the trend line of other points. The first crack tensile strain was about 249 micro-strain at the quasi-static strain rate and decreased to 215 micro-strain at the rate of 1×10^{-1} s^{-1}. Except at the rate of 1×10^{-3} s^{-1}, the ratio of the dynamic to the static first tensile cracking strain versus the tensile strain rate can be modeled well as follows:

$$\varepsilon_{\mathrm{fct}} / \varepsilon_{\mathrm{fcts}} = 1.0 - 0.02955\log\frac{\dot{\varepsilon}_{\mathrm{t}}}{\dot{\varepsilon}_{\mathrm{ts}}}, \quad 4\times10^{-6}\ \mathrm{s}^{-1} < \dot{\varepsilon}_{\mathrm{t}} \le 10^{-1}\ \mathrm{s}^{-1},\ R^2 = 0.99996, \tag{2}$$

where $\varepsilon_{\mathrm{fcts}}$ denotes the first crack tensile strain under a quasi-static loading rate, and $\varepsilon_{\mathrm{fct}}$ denotes the first crack tensile strain under the strain rate of $\dot{\varepsilon}_{\mathrm{t}}$.

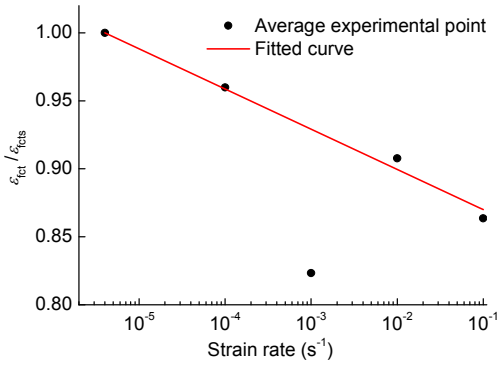


Fig. 5 Dynamic decrease effect of first crack tensile strain of UHTCC

A plot of the first crack tensile strength versus strain rates curve is presented in Fig. 6, where σ_{fcts} denotes the quasi-static tensile first crack strength, and σ_{fct} denotes the first crack tensile strength under the strain rate $\dot{\varepsilon}_{\mathrm{t}}$. The first crack tensile strength was also rate dependent. When the strain rates increased, the first crack tensile strength tended to increase overall. The first crack tensile strength at the rate of 1×10^{-1} s^{-1} was about 1.36 times that at the quasi-static strain rate. The strain rate of 1×10^{-3} s^{-1} looks like a threshold after which the dynamic first tensile crack strength increases much faster and almost linearly with strain rate in the semi-logarithmic coordinates (Fig. 6).

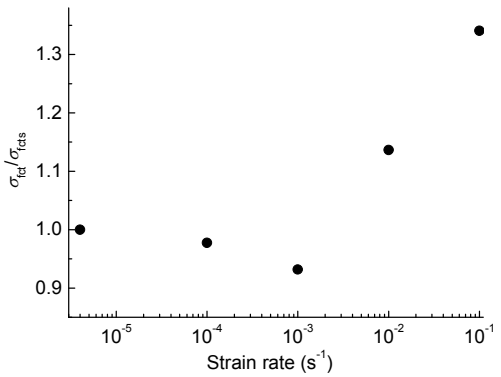


Fig. 6 Dynamic increase effect of first crack tensile strength of UHTCC

The physical explanation of the dynamic increase effect of first crack tensile strength may be similar to that of the tensile strength of concrete (Yan *et al.*, 2005). With increasing strain rate, crack formation and propagation become so rapid that there is insufficient time for the crack to propagate along the weakest section of the specimen. This leads to an increase in first crack tensile strength of the UHTCC. The chemical bond at the PVA fiber/matrix interface may also have an influence on the dynamic first crack tensile strength, but further investigation is needed to confirm this.

3.5 Rate dependencies of the ultimate tensile strength and strain

The dynamic ultimate tensile strain to quasi-static ultimate tensile strain ratios under different strain rates are presented in Table 3. At all strain rates, the dynamic ultimate tensile strain ($\varepsilon_{\mathrm{ut}}$) to static ultimate tensile strain ($\varepsilon_{\mathrm{uts}}$) ratios all lay in the range of 0.95 to 1.03, which means that the ultimate

tensile strain was rate independent. This independency may be due to the flexibility and good bridging ability of PVA fibers.

Table 3 Comparison of the ultimate tensile strains under different strain rates

Strain rate	$\varepsilon_{ut}/\varepsilon_{uts}$
4×10^{-6}	1.00
1×10^{-5}	1.00
1×10^{-4}	1.03
1×10^{-3}	0.97
1×10^{-2}	1.03
1×10^{-1}	0.95

The dynamic ultimate tensile strength to quasi-static ultimate tensile strength ratios versus strain rates curves are plotted in Fig. 7. It is obvious that the ultimate tensile strength was rate dependent. The ultimate tensile strength tended to increase slowly when the strain rate increased from quasi-static to about 1×10^{-3} s^{-1}, and increased at a significantly higher rate when the strain rate continued to increase. The ultimate tensile strength at 1×10^{-1} s^{-1} was about 1.40 times that at the quasi-static rate. For simplicity, the experimental curve was modeled as follows:

$$\sigma_{ut}/\sigma_{uts}=\begin{cases}1.0+0.03345\log\dfrac{\dot{\varepsilon}_t}{\dot{\varepsilon}_{ts}}, \\ \qquad 4\times10^{-6}\ s^{-1}\le\dot{\varepsilon}_t\le10^{-3.29238}\ s^{-1}, \\ 0.75645+0.14912\log\dfrac{\dot{\varepsilon}_t}{\dot{\varepsilon}_{ts}}, \\ \qquad 10^{-3.29238}\ s^{-1}<\dot{\varepsilon}_t\le10^{-1}\ s^{-1},\end{cases} \quad (3)$$

where σ_{uts} denotes the ultimate tensile strength under the quasi-static strain rate, and σ_{ut} denotes the dynamic ultimate tensile strength.

3.6 Rate dependency of energy absorption capacity

The energy absorption capacity is an essential parameter for the application of UHTCC in earthquake resistant structures. It can be defined as the area under the stress-strain curve up to the peak stress. Table 4 presents the energy absorption capacity at all strain rates. The experimental results for concrete from Yan *et al*. (2005) are also shown for comparison. The energy adsorption capacities showed little difference when the strain rates were lower than 1×10^{-4} s^{-1}, and tended to increase continuously when the strain rates increased. The energy adsorption capacity under the strain rate of 1×10^{-1} s^{-1} was about 1.36 times that under the quasi-static rate. The capacity increase was due mainly to the increase in ultimate tensile strength. The energy adsorption capacity of UHTCC was about 3000 times that of C10 concrete and 1000 times that of C20 concrete, which means that the UHTCC has a great advantage over concrete in seismic-resistant engineering applications.

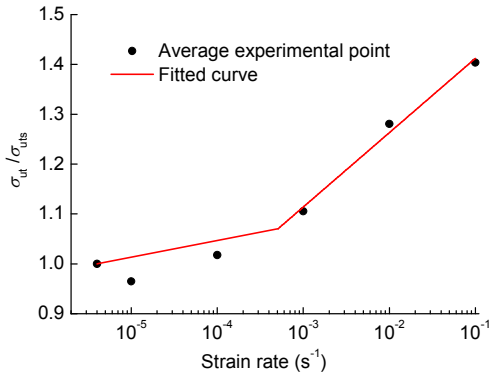


Fig. 7 Dynamic increase effect of ultimate tensile strength of UHTCC

Table 4 Energy absorption capabilities of UHTCC and concrete under different strain rates

Strain rate (s^{-1})	Energy adsorption capacity (N/m^2)		
	UHTCC	Concrete C10 (Yan *et al.*, 2005)	Concrete C20 (Yan *et al.*, 2005)
4×10^{-6}	189 392	–	–
1×10^{-5}	168 109	52.7	133.8
1×10^{-4}	188 175	68.7	135.7
1×10^{-3}	196 365	69.3	207.0
1×10^{-2}	239 658	77.7	218.7
1×10^{-1}	257 240	88.4	228.0

4 Conclusions

Based on uniaxial tensile tests on 2D thin plate specimens of UHTCC with strain rates ranging from 4×10^{-6} s^{-1} to 1×10^{-1} s^{-1}, the following main conclusions can be drawn:

1. Under all the strain rates considered, the first crack tensile strain, first crack tensile strength, elastic modulus, ultimate tensile strength, and energy absorption capability of the UHTCC were all rate dependent. Except for the first crack tensile strain, which showed a dynamic decrease effect, all others showed significant dynamic increase effects. Under the highest strain rate of 1×10^{-1} s^{-1}, the first crack tensile strain, first crack tensile strength, elastic modulus, ultimate tensile strength, and energy adsorption capability were respectively 0.86, 1.34, 1.49, 1.40, and 1.36 times those under the static rate.

2. The multiple cracking modes and ultimate tensile strain capacity of the UHTCC were both approximately rate independent. All the UHTCC specimens showed obvious saturated multiple cracking behaviors, with the average ultimate crack width consistently below 100 μm and the ultimate tensile strain around 3.7%.

3. The strain rate of 1×10^{-3} s^{-1} seems to be the threshold for dynamic increase effects of first crack tensile strength, elastic modulus, ultimate tensile strength, and energy absorption capacity of UHTCC. Their dynamic increase effects were not pronounced until the strain rate was higher than 1×10^{-3} s^{-1}.

4. UHTCC shows a great advantage over concrete in energy absorption capacity. Under seismic loads, the energy absorption capacity of UHTCC is about 1000 times that of C20 concrete.

Above all, the application of UHTCC in seismic engineering is well worth exploring. If necessary, special construction technologies may be adopted to guarantee a generally 2D distribution of fibers to make full use of the fiber reinforcing effect.

References

Boshoff, W.P., van Zijl, G.P.A.G., 2007. Time-dependent response of ECC: characterisation of creep and rate dependence. *Cement and Concrete Research*, **37**(5):725-734. http://dx.doi.org/10.1016/j.cemconres.2007.02.001

Douglas, K.S., Billington, S.L., 2011. Strain rate dependence of HPFRCC cylinders in monotonic tension. *Materials and Structures*, **44**(1):391-404. http://dx.doi.org/10.1617/s11527-010-9634-4

Fischer, G., 2002. Behavior of Reinforced ECC Flexural Members under Reversed Cyclic Loading Conditions. PhD Thesis, University of Michigan, Michigan, USA.

Fischer, G., Li, V.C., 2002. Influence of matraix ductility on tension-stiffening behavior of steel reinforced engineered cementitious composites (ECC). *Structural Journal*, **99**(1):104-111. http://dx.doi.org/10.14359/11041

Li, H., Xu, S., 2011. Determination of energy consumption in the fracture plane of ultra high toughness cementitious composite with direct tension test. *Engineering Fracture Mechanics*, **78**(9):1895-1905. http://dx.doi.org/10.1016/j.engfracmech.2011.03.012

Li, V.C., 1997. Damage tolerance of engineered cementitious composites. Proceedings of the 9th International Conference of Fracture, Sydney, Australia. Pergamon, Oxford, UK, p.619-630.

Li, V.C., Leung, C.K.Y., 1992. Steady state and multiple cracking of short random fiber composites. *Journal of Engineering Mechanics*, **118**(11):2246-2264. http://dx.doi.org/10.1061/(asce)0733-9399(1992)118:11(2246)

Li, V.C., Hashida, T., 1993. Engineering ductile fracture in brittle matrix composites. *Journal of Materials Science Letters*, **12**(12):898-901. http://dx.doi.org/10.1007/BF00455611

Li, V.C., Kanda, T., 1998. Innovations forum: engineered cementitious composites for structural applications. *Journal of Materials in Civil Engineering*, **10**(2):66-69. http://dx.doi.org/10.1061/(asce)0899-1561(1998)10:2(66)

Maalej, M., Quek, S.T., Zhang, J., 2005. Behavior of hybrid-fiber engineered cementitious composites subjected to dynamic tensile loading and projectile impact. *Journal of Materials in Civil Engineering*, **17**(2):143-152. http://dx.doi.org/10.1061/(asce)0899-1561(2005)17:2(143)

Malvar, L.J., Ross, C.A., 1998. Review of strain rate effects for concrete in tension. *Materials Journal*, **95**(6):735-739. http://dx.doi.org/10.14359/418

Mechtcherine, V., Silva, F.A., Butler, M., *et al*., 2011. Behavior of strain-hardening cement-based composites under high strain rates. *Journal of Advanced Concrete Technology*, **9**(1):51-62. http://dx.doi.org/10.3151/jact.9.51

Reinhardt, H.W., 1985. Strain rate effects on the tensile strength of concrete as predicted by thermodynamic and fracture mechanics models. *Materials Research Society Symposia Proceedings*, **64**:1-13. http://dx.doi.org/10.1557/PROC-64-1

Ross, C.A., Tedesco, J.W., Kuennen, S.T., 1995. Effects of strain rate on concrete strength. *Materials Journal*, **92**(1):37-47. http://dx.doi.org/10.14359/1175

Rossi, P., van Mier, J.G.M., Toutlemonde, F., *et al.*, 1994. Effect of loading rate on the strength of concrete subjected to uniaxial tension. *Materials and Structures*, **27**(5):260-264. http://dx.doi.org/10.1007/BF02473042

Xiao, S.Y., Lin, G., Wang, Z., *et al.*, 2001. Effects of strain rate on dynamic behavior of concrete in tension. *Journal of Dalian University of Technology*, **41**(6):721-725 (in Chinese).

Xu, S., Li, H., 2009. Uniaxial tensile experiments of ultra high toughness cementitious composite. *China Civil Engineering Journal*, **42**(9):32-41 (in Chinese).

Xu, S., Cai, X., 2010. Experimental study and theoretical models on compressive properties of ultrahigh toughness cementitious composites. *Journal of Materials in Civil Engineering*, **22**(10):1067-1077. http://dx.doi.org/10.1061/(ASCE)MT.1943-5533.0000109

Yan, D., Lin, G., Wang, Z., *et al.*, 2005. A study on direct tensile properties of concrete at different strain rates. *China Civil Engineering Journal*, **38**(6):97-103 (in Chinese).

Yang, E., Li, V.C., 2006. Rate dependences in engineered cementitious composite. *In*: Fischer, G., Li, V.C. (Eds.), International RILEM Workshop on High Performance Fiber Reinforced Cementitious Composites in Structural Applications. RILEM Publications SARL, Bagneux, France, p.83-92.

Yang, E., Li, V.C., 2012. Tailoring engineered cementitious composites for impact resistance. *Cement and Concrete Research*, **42**(8):1066-1071. http://dx.doi.org/10.1016/j.cemconres.2012.04.006

中文概要

题　目：超高韧性水泥基复合材料直接拉伸特性应变率效应研究

目　的：水泥基材料的拉伸性能会随着荷载速率的变化而变化。本文旨在探讨加载速率为 4×10^{-6}~1×10^{-1} s^{-1} 时，超高韧性水泥基复合材料直接拉伸初裂抗拉强度、初裂抗拉应变、弹性模量、极限抗拉应变、极限抗拉强度、多缝开裂特性和耗能能力的变化规律，为超高韧性水泥基复合材料在抗震工程中的应用提供必要的科学依据和参考。

创新点：1. 通过直接拉伸试验较为全面地测定超高韧性水泥基复合材料在 4×10^{-6}~1×10^{-1} s^{-1} 应变速率范围内的直接拉伸性能；2. 建立适宜的拟合方程，可直观反映多种直接拉伸性能指标随应变率的变化规律。

方　法：1. 通过直接拉伸试验，确定加载速率对超高韧性直接拉伸特性的影响（图 2 和 4）；2. 通过对实验结果的拟合，简单直观地反映应变率对拉伸弹性模量、初裂抗拉强度和极限抗拉强度的影响规律（图 3、5 和 7）。

结　论：基于超高韧性水泥基复合材料薄板直接拉伸试验，当应变速率在 4×10^{-6}~1×10^{-1} s^{-1} 的范围内变化时：1. 材料的初裂抗拉强度、初裂抗拉应变、拉伸弹性模量、极限抗拉强度和耗能能力都具有应变速率敏感性，其中除初裂抗拉应变随应变率升高而减小外，其它几项性能指标都显示出明显的动态强化效应；2. 多缝开裂模式和极限抗拉应变对应变率不敏感，极限裂缝宽度始终在 100 μm 以内，极限抗拉应变保持在 3.7%左右；3. 应变率对初裂抗拉强度、拉伸弹性模量、极限抗拉强度和耗能能力的动态增强效应都存在一个阈值（皆在 1×10^{-3} s^{-1} 附近），在应变率达到阈值之后，动态效应才更加显著；4. 超高韧性水泥基复合材料具有明显优于混凝土的耗能能力，在地震荷载（对应应变率在 1×10^{-4}~1×10^{-2} s^{-1}）作用下其耗能能力可达 C20 混凝土的 1000 倍。

关键词：超高韧性水泥基复合材料；率效应；直接拉伸；应变硬化；多缝开裂